Journal of Solid State Chemistry 184 (2011) 1820–1827

Contents lists available at ScienceDirect

Journal of Solid State Chemistry

journal homepage: www.elsevier.com/locate/jssc

Synthesis of mesoporous zeolite single crystals with cheap porogens

Haixiang Tao [1], Changlin Li [1], Jiawen Ren, Yanqin Wang *, Guanzhong Lu *

Key Laboratory for Advanced Materials, Research Institute of Industrial Catalysis, East China University of Science and Technology, Shanghai 200237, PR China

ARTICLE INFO

Article history:
Received 25 November 2010
Received in revised form
8 May 2011
Accepted 18 May 2011
Available online 26 May 2011

Keywords:
Mesoporous zeolite
Porogen
Single crystal
Catalytic activity

ABSTRACT

Mesoporous zeolite (silicalite-1, ZSM-5, TS-1) single crystals have been successfully synthesized by adding soluble starch or sodium carboxymethyl cellulose (CMC) to a conventional zeolite synthesis system. The obtained samples were characterized by X-ray diffraction (XRD), Fourier transform infrared spectroscopy (FT-IR), scanning electron microscopy (SEM), transmission electron microscopy (TEM), nitrogen sorption analysis, ^{27}Al magic angle spinning nuclear magnetic resonance (^{27}Al MAS NMR), temperature-programmed desorption of ammonia (NH_3-TPD) and ultraviolet–visible spectroscopy (UV–vis). The SEM images clearly show that all zeolite crystals possess the similar morphology with particle size of about 300 nm, the TEM images reveal that irregular intracrystal pores are randomly distributed in the whole crystal. ^{27}Al MAS NMR spectra indicate that nearly all of the Al atoms are in tetrahedral co-ordination in ZSM-5, UV–vis spectra confirm that nearly all of titanium atoms are incorporated into the framework of TS-1. The catalytic activity of meso-ZSM-5 in acetalization of cyclohexanone and meso-TS-1 in hydroxylation of phenol was also studied. The synthesis method reported in this paper is cost-effective and environmental friendly, can be easily expended to prepare other hierarchical structured zeolites.

1. Introduction

Mesoporous zeolite materials are hierarchical porous solids that combined the advantages of both zeolites and mesoporous materials. They can not only maintain the stability and strong acidity but also overcome the diffusion limitation of zeolites. They have been proven to be promising catalysts for the alkylation of benzene with ethane, the cracking of 1,3,5-triisopropylbenzene and cumene, the esterification reaction between benzyl alcohol and hexanoic acid, and so on [1–4]. Up to now, various attempts have been used to synthesize mesoporous zeolites [5,6]. Among all the synthetic methods, there are two basic routes: one is to generate mesopores by treating synthesized zeolites [7,8], such as steaming, acid or alkaline leaching. This method is very simple, but lack of control in generated mesopores. A recent report shows that partial detemplation and desilication can enhance the tailored degree of mesoporosity [9], which will promote the application of this method. The other is to synthesize by templating method. In a typical procedure, the mesopores are generated by the removal of auxiliary templates encapsulated in the zeolite during growth. Due to the special growth mechanism of zeolite materials, the conventional surfactants used in the synthesis of mesoporous materials are not valid in producing mesopores in zeolites. Therefore, selecting suitable template is crucial. Since Jacobsen et al. [10] first reported the preparation of mesoporous zeolite by using carbon particles as a template, many other hard templates, such as carbon nanotube [11], carbon nanofiber [12], carbon aerogels [13,14] and mesoporous carbon [15,16] have been used. Furthermore, some special polymers and supramolecular templates had strong interaction with silica were also used as templates to simplify the synthesis. For example, Wang and Pinnavaia [17] prepared MFI zeolite with small and uniform intracrystal mesopores by using silylated polyethylenimine as template. Xiao et al. [18] synthesized hierarchical mesoporous beta and ZSM-5 by using mesoscale cationic polymers as template. Ryoo et al. [19] obtained mesoporous zeolites with tunable pore size by using organosilane surfactants as supermolecular template. However, most of the templates are expensive and not easily available, result in hampering in their industrial applications. To the best of our knowledge, the synthesis of structure-controllable hierarchical zeolite with cheap and easily available templates was rarely reported. In recent years, several natural resources have been used to synthesize porous materials, for example, Mann et al. [20] fabricated zeolite materials with a hierarchical micro/meso/macrospore organization by using silicalite nanoparticles and starch gel as templates. Bao et al. [21] reported the synthesis of mesopore-modified ZSM-5 zeolites with hierarchical porous structure via adopting tetrapropylammonium hydroxide and starch as co-templates. Xiao et al. [22] obtained

* Corresponding authors. Fax: +86 21 64253824.
E-mail addresses: wangyanqin@ecust.edu.cn (Y. Wang), gzhlu@ecust.edu.cn (G. Lu).
[1] Both authors contribute to this work equally.

0022-4596/$ - see front matter Crown Copyright © 2011 Published by Elsevier Inc. All rights reserved.
doi:10.1016/j.jssc.2011.05.023

a hierarchical mesoporous ZSM-5 zeolite by using starch-derived bread as a meso-template.

Here, we also present a facile method by using cheap templates to synthesize mesoporous zeolite single crystal. Soluble starch is a nontoxic, harmless, biodegradable and environmental-friendly renewable natural resource. Sodium carboxymethyl cellulose (CMC) is a derivation of natural cellulose. Both of them are cheap, stable, and have been used in various fields. In this work, they are directly added to the synthesis system as meso-porogen and different type of mesoporous zeolite (silicalite-1, ZSM-5, TS-1) single crystals have been successfully synthesized.

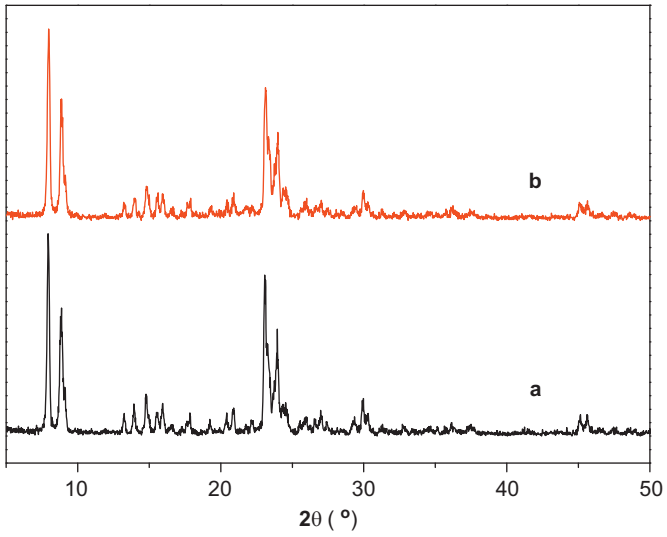

Fig. 1. XRD patterns of mesoporous silicalite-1: (a) S-Silicalite-1 and (b) C-Silicalite-1.

2. Experimental

2.1. Synthesis

The synthesis of mesoporous zeolite was conducted directly under hydrothermal conditions. All the reagents including tetrapropylammonium hydroxide (TPAOH, 20–25 wt%), tetraethyl orthosilicate (TEOS), NaOH, $NaAlO_2$, tetrabutylorthotitanate (TBOT), acetylacetone, soluble starch, sodium carboxymethyl cellulose (CMC) were reagent grade and used without further purifications.

2.1.1. Synthesis of mesoporous zeolites using soluble starch as porogen

In a typical synthesis of mesoporous silicalite-1, 0.032 g of NaOH, 4.8 g of TPAOH, 4.2 g of TEOS and 10.8 g of deionized water were mixed and stirred at 353 K for 4 h, then, 2 g of soluble starch was added. After stirring at 353 K overnight, the mixture was transferred into an autoclave and aged at 453 K for 2 d for further crystallization. The product was collected by filtration, dried in air and calcined at 873 K for 10 h. The obtained mesoporous silicalite-1 was designated as S-Silicalite-1. Furthermore, mesoporous ZSM-5 and mesoporous TS-1 were also synthesized with the similar procedure by introducing aluminum (0.083 g $NaAlO_2$, Si/Al=20) and titanium source (0.174 g TBOT, Si/Ti=40) in the initial synthesis composition. They were designated as S-ZSM-5 and S-TS-1, respectively.

2.1.2. Synthesis of mesoporous zeolites using CMC as porogen

In a typical synthesis of mesoporous silicalite-1, 0.032 g of NaOH, 4.8 g of TPAOH, 4.2 g of TEOS and 10.8 g of deionized water were mixed and stirred at 353 K for 4 h, then, 1.2 g of CMC was added. The other procedures are the same as above. The obtained mesoporous silicalite-1 was designated as C-Silicalite-1. Furthermore, mesoporous ZSM-5 and mesoporous TS-1 were synthesized

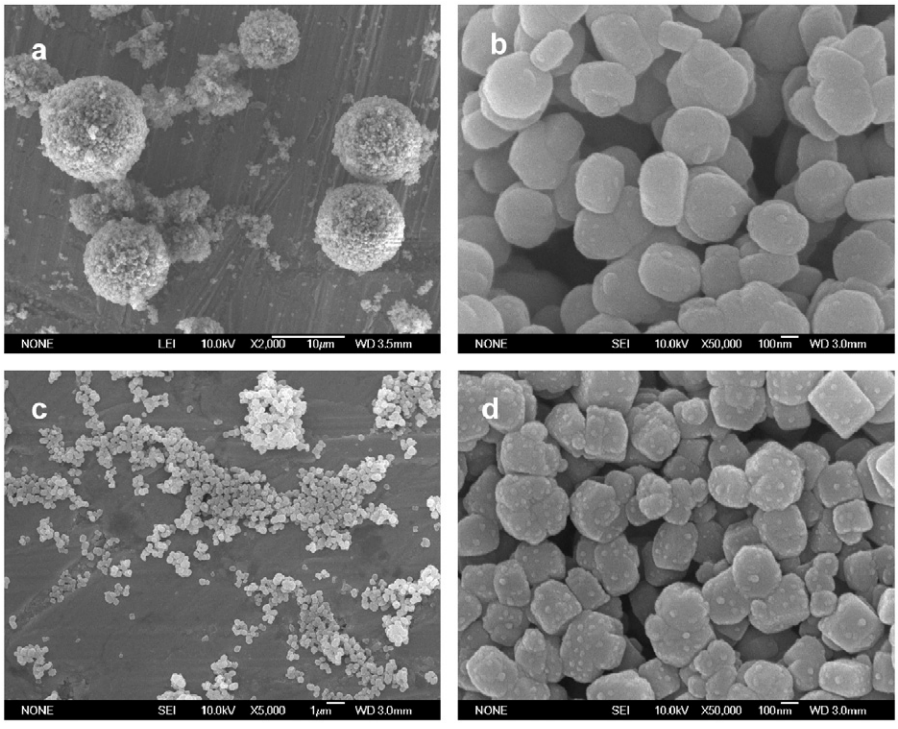

Fig. 2. SEM images of mesoporous silicalite-1: (a, b) S-Silicalite-1 and (c, d) C-Silicalite-1.

with the similar procedure by introducing aluminum (0.083 g $NaAlO_2$, Si/Al=20) and titanium source (0.174 g TBOT, Si/Ti=40) in the initial synthesis composition. They were designated as C-ZSM-5 and C-TS-1, respectively.

2.2. Characterization

X-ray powder diffraction (XRD) patterns were recorded on a Bruker diffractometer with Cu $K\alpha$ radiation (λ=1.5418 Å). The scanning electron microscopy (SEM) was collected on a JSM-7401F scanning electron microscope with an operating voltage at 10 kV. The transmission electron microscopy (TEM) was carried out on a Tecnai 20 S-TWIN instrument operating at 200 kV. The high-resolution transmission electron microscopy (HR-TEM) and selected area electron diffraction were recorded on JEM-2010 instrument operating at 200 kV. The nitrogen adsorption experiment was measured on a Micromeritics ASAP 2020M sorption analyzer. Before the measurements, the samples were outgassed at 573 K for 8 h. ^{27}Al MAS NMR spectra were obtained on a Bruker DRX-400 Spectrometer equipped with a magic angle spin probe at room temperature. Pyridine-adsorbed FT-IR spectra were carried out on a Nicolet Model 710, each sample was grounded into fine powders and pressed into a very thin self-supporting wafer. The disc was mounted in a quartz IR cell equipped with a CaF_2 window and a vacuum system. Prior to adsorption, the sample disc was pretreated in situ at 673 K for 2 h under evacuation, then cooled to 323 K where pyridine vapor was introduced into the cell for 0.5 h. The physically adsorbed pyridine was removed by evacuating for 1 h, after that, the sample was heated in vacuum for 1 h at 373 K, and a spectrum was recorded. Temperature-programmed desorption of ammonia (NH_3-TPD) was performed on an apparatus PX200 (Tianjin Golden Eagle Technology Limited Corporation). The sample (100 mg) was pretreated at 773 K for 2 h and then cooled down to 323 K under a N_2 flow. Pure NH_3 was injected until adsorption saturation was reached, followed by a flow of N_2 for 1 h. Then the temperature was raised from 363 to 873 K with a heating rate of 10 K min^{-1} and the amount of desorbed ammonia was detected by using thermal conductivity detector (TCD) at 383 K. Diffuse reflectance ultraviolet–visible (UV–vis) spectra were recorded under ambient conditions on a SHIMADZU UV-2550 spectrometer.

2.3. Catalyst evaluation

2.3.1. Acetalization of cyclohexanone

The acetalization of cyclohexanone was carried out batch-wise in a round-bottomed flask equipped with a condenser and a magnetic stirrer. In a typical reaction, 50 mg of catalyst (H^+ form) was dispersed in a solution containing 10 mL of methanol and 0.098 g of cyclohexanone. The solution was stirred at 323 K for 4 h. The reaction mixtures were separated by centrifugation and analyzed by a Perkin-Elmer Clarus 500 gas chromatography with a SE-54 column. The product was further confirmed by GC–MS.

2.3.2. Hydroxylation of phenol

The hydroxylation of phenol was carried out batch-wise in a round-bottomed flask equipped with a condenser and a magnetic stirrer. Typically, 0.94 g of phenol was mixed with 30 g of deionized water containing 0.5 g of TS-1 sample, then required amount of hydrogen peroxide (30 wt%) was added, the mixture was stirred at 353 K for 2 h. Finally, the mixture was separated by

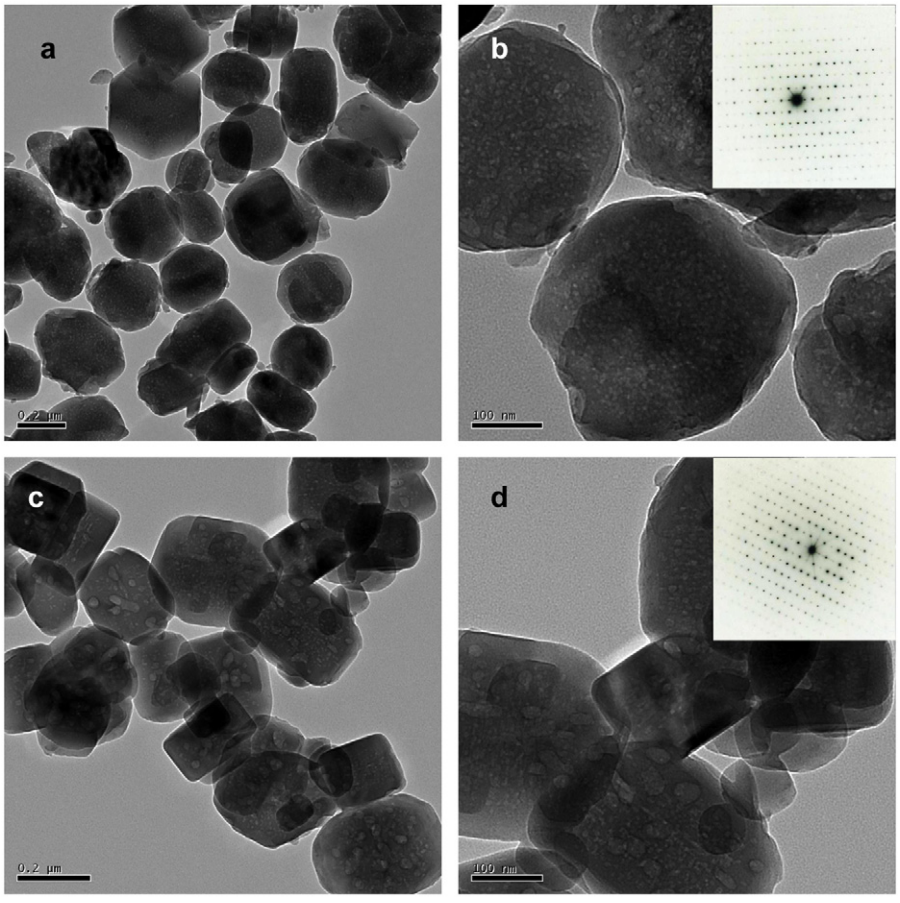

Fig. 3. TEM images of mesoporous silicalite-1: (a, b) S-Silicalite-1 and (c, d) C-Silicalite-1.

centrifugation and analyzed by an HPLC apparatus (Agilent 1200 Series) equipped with an XDB-C18 column (Eclipse USA).

3. Results and discussion

Soluble starch and CMC are macromolecules containing many hydroxyl groups on their long chains, which endow them the capability to enhance the interface interaction. So they can be used as adhesive, thickening agent, and so on. In our synthesis, they were integrated into the zeolite through the hydrogen bond interaction between Si-OH and the hydroxyl groups on macromolecules, after calcination at high temperature, the porogens were removed and the mesoporous zeolite was obtained.

Fig. 1 shows the XRD patterns of mesoporous silicalite-1 synthesized by two different porogens. It is clearly seen that both samples show well-resolved peaks in the range of 5–50°, which can be indexed to the characteristic diffractions of MFI zeolite structure. No trace of amorphous background and the line broadening in the peaks indicate the high crystallinity of zeolites. It can be concluded from the XRD results that different porogens used in the synthesis has little effect on the crystallization of silicalite-1.

Fig. 2 presents the morphology of mesoporous silicalite-1. The SEM images at low magnification show that these two samples exhibit different aggregation states. S-Silicalite-1 is spherical aggregates in micrometer, whereas C-Silicalite-1 is well-dispersed zeolite particles. However, the high magnification SEM images reveal that both zeolites possess the similar morphology with particle size of about 300 nm. Interestingly, S-Silicalite-1 possesses smooth surface, which is similar to the conventional silicalite-1, but there are many small nanoparticles adhered on the surface of C-Silicalite-1.

The representative TEM images (Fig. 3) and selected area electron diffraction patterns (Fig. 3 inset) indicate that both of the final Silicalite-1 is mesoporous MFI zeolites with single-crystalline framework rather than polycrystalline framework. The overview of TEM images shows that well-shaped zeolites with uniform size are obtained, and many brighter areas corresponding to the mesopores created by the removal of porogens distributed homogenously in each of the single crystals. Typically, the size of mesopore is below 10 nm for S-Silicalite-1. However, for C-Silicalite-1, besides the small mesopores below 10 nm, there are some irregular larger mesopores. The formation of these larger mesopores may be due to the lack of mix and swollen of the CMC in the composite. In fact, the mixture contained CMC is very pasty, and hard to stir.

The hierarchical porosity of zeolites is further demonstrated by N_2 sorption. However, both isotherms show a step at a relative pressure P/P_0 of 0.2–0.4 in Fig. 4, this hysteresis loop does not reveal any real pores, this hysteresis loop can be ascribed to a fluid-to-crystal-like phase transition of nitrogen molecules in the micropores or high-quality zeolite crystal, which has been reported in the previous reports [14,23,24]. Argon sorption isotherms (not given here) also confirm the inexistence of the pores in the range of 0.2–0.4. The parameters of the pore structure are given in Table 1. It is clear that both samples possess large surface area, similar to the conventional Silicalite-1, but the values of the pore volume are higher than the typical values for Silicalite-1, which is due to the presence of additional mesopores in the samples.

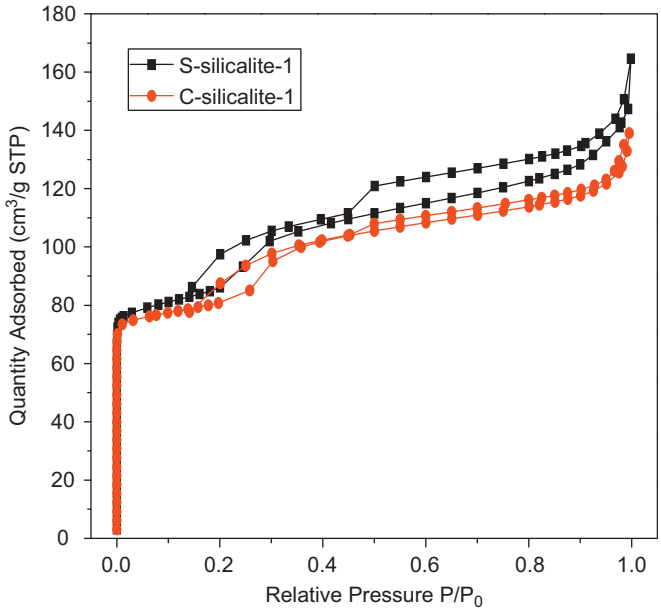

Fig. 4. N_2 adsorption-desorption isotherms of mesoporous silicalite-1.

Besides mesoporous silicalite-1, other MFI-type mesoporous molecular sieves were also synthesized by this method. Fig. 5 shows the XRD patterns of (a) S-ZSM-5-20, (b) S-TS-1, (c) C-ZSM-5-20 and (d) C-TS-1. It is noted that all samples show the characteristic diffraction peaks of MFI topology. Their specific structural parameters can be seen from Table 1.

SEM images in Fig. 6 reveal that mesoporous zeolites synthesized with different porogens have similar morphology. Mesoporous ZSM-5 is composed of nano-particle aggregates without observable amorphous structure. Mesoporous TS-1 is composed of the uniform, regular nanoparticles with size about 250 nm.

Fig. 7 shows the TEM images of mesoporous ZSM-5 and TS-1, the individual zeolite particles have regular shape with a size around 250 nm are observed, which are similar to silicalite-1.

Table 1
Textural properties of mesoporous MFI zeolites.

Samples	S_{BET} ($m^2\,g^{-1}$)	S_{micro} ($m^2\,g^{-1}$)[a]	S_{exter} ($m^2\,g^{-1}$)	V_{tol} ($cm^3\,g^{-1}$)	V_{micro} ($cm^3\,g^{-1}$)[a]	V_{meso} ($cm^3\,g^{-1}$)
S-Silicalite-1	292	75	218	0.23	0.04	0.19
S-ZSM-5-20	338	232	107	0.20	0.11	0.09
S-ZSM-5-50	320	156	164	0.20	0.08	0.12
S-ZSM-5-100	329	152	178	0.23	0.07	0.16
S-TS-1	378	278	100	0.22	0.12	0.10
C-Silicalite-1	274	167	106	0.22	0.08	0.14
C-ZSM-5-20	321	65	256	0.23	0.04	0.19
C-ZSM-5-50	347	163	184	0.22	0.07	0.15
C-ZSM-5-100	316	118	198	0.22	0.06	0.16
C-TS-1	253	69	184	0.16	0.04	0.12

[a] Determined by the t-Plot method.

The SAED patterns (Fig. 7b and e inset) of mesoporous ZSM-5 confirm that mesoporous ZSM-5 particle is a single crystal. The high-resolution TEM images of mesoporous ZSM-5 are taken from the edge of each selected crystal, the lattice fringes are clearly distinguishable, revealing high crystallinity of mesoporous ZSM-5, which is consistent with XRD patterns. The ordered micropores and channels are well arranged in the crystal. On the other hand, the irregular intracrystal mesopores are randomly distributed in the whole crystal. It is interesting to note that the pore structure in samples synthesized by using the same porogen is different. It may be due to the influence of pH value, viscosity and crystallization character at different synthesis system. Actually, the viscosity of the synthesis system is low, and the pH value is gradually decreased when using soluble starch as porogen; while the viscosity increases and the pH value keeps constant when using CMC as porogen. The further experimental results show that many factors, including the amount of water, alkali and template and even aging temperature, have effect on the results of the synthesis, such as phase composition and mesoporous structure. In the synthesis, less water leads to the generation of hybrid phases and even to non-crystallinity, but if too much water is added, the mesopores are not generated because excessive water inhibits the integration of template into zeolite. Excessive alkali induces the formation of hybrid phase, while less alkali decreases the crystallinity of zeolite. The addition of template has an effect on the pH value and viscosity, which is also responsible for phase composition and mesoporous structure of zeolite.

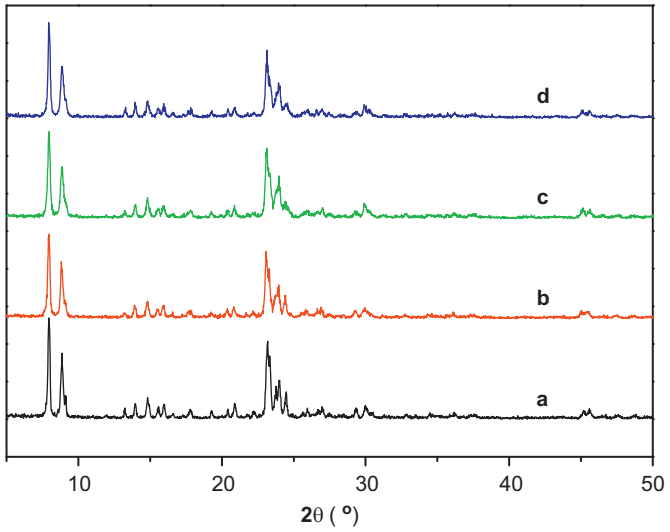

Fig. 5. XRD patterns of mesoporous MFI zeolites: (a) S-ZSM-5; (b) S-TS-1; (c) C-ZSM-5 and (d) C-TS-1.

The co-ordination states of hybrid atoms in the samples are characterized by solid state NMR and UV–vis spectroscopy. Fig. 8 shows the ^{27}Al MAS NMR spectra of mesoporous ZSM-5 (Si/Al=20). Each spectrum has only one sharp signal at 54 ppm, which confirms that all aluminum atoms are incorporated into the zeolite framework at 4-coordinate state and different porogens have no influence on the incorporation state of aluminum species. The species of Ti in mesoporous TS-1 (Si/Ti=40) was probed by UV–vis spectra. As shown in Fig. 9, the strong signal at 209 nm confirms the tetra-coordinate titanium species exist in S-TS-1, which is similar to conventional TS-1. However, for C-TS-1, besides the main resonance at 209 nm, there is another weak signal at 320 nm, which is considered as the existence of anatase TiO_2.

The temperature-programmed desorption of ammonia for samples with various Si/Al ratios was measured to characterise the acidity of the mesoporous zeolite (H^+form) (Fig. 10). All samples show two desorption peaks, the low temperature desorption peak indicates weak adsorption acidic sites, and the peak at high temperature is attributed to the interaction of NH_3 with strong acidic sites. The intensity of each peak decreased as increasing Si/Al ratio. Pyridine-adsorbed FT-IR spectroscopy spectra in 1400–1600 cm^{-1} for samples with various Si/Al ratio are shown in Fig. 11. There are three bands in the region. The one at about 1450 cm^{-1} arising from the C–C stretch of a coordinatively bonded pyridine complex indicates the presence of Lewis acid sites. The 1540 cm^{-1} one is attributed to the C–C stretching

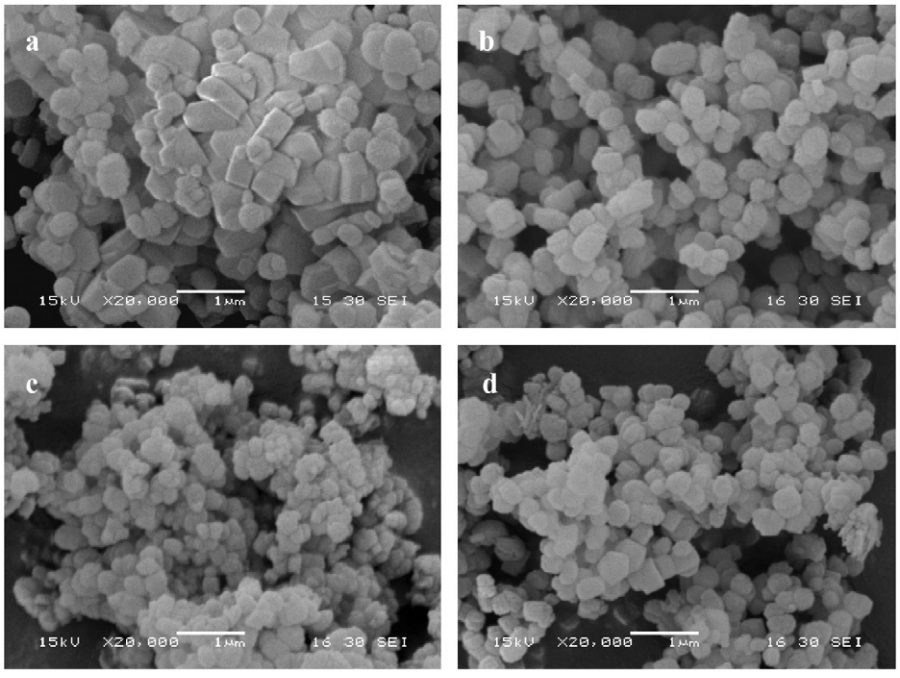

Fig. 6. SEM images of mesoporous MFI zeolites: (a) S-ZSM-5, (b) S-TS-1, (c) C-ZSM-5 and (d) C-TS-1.

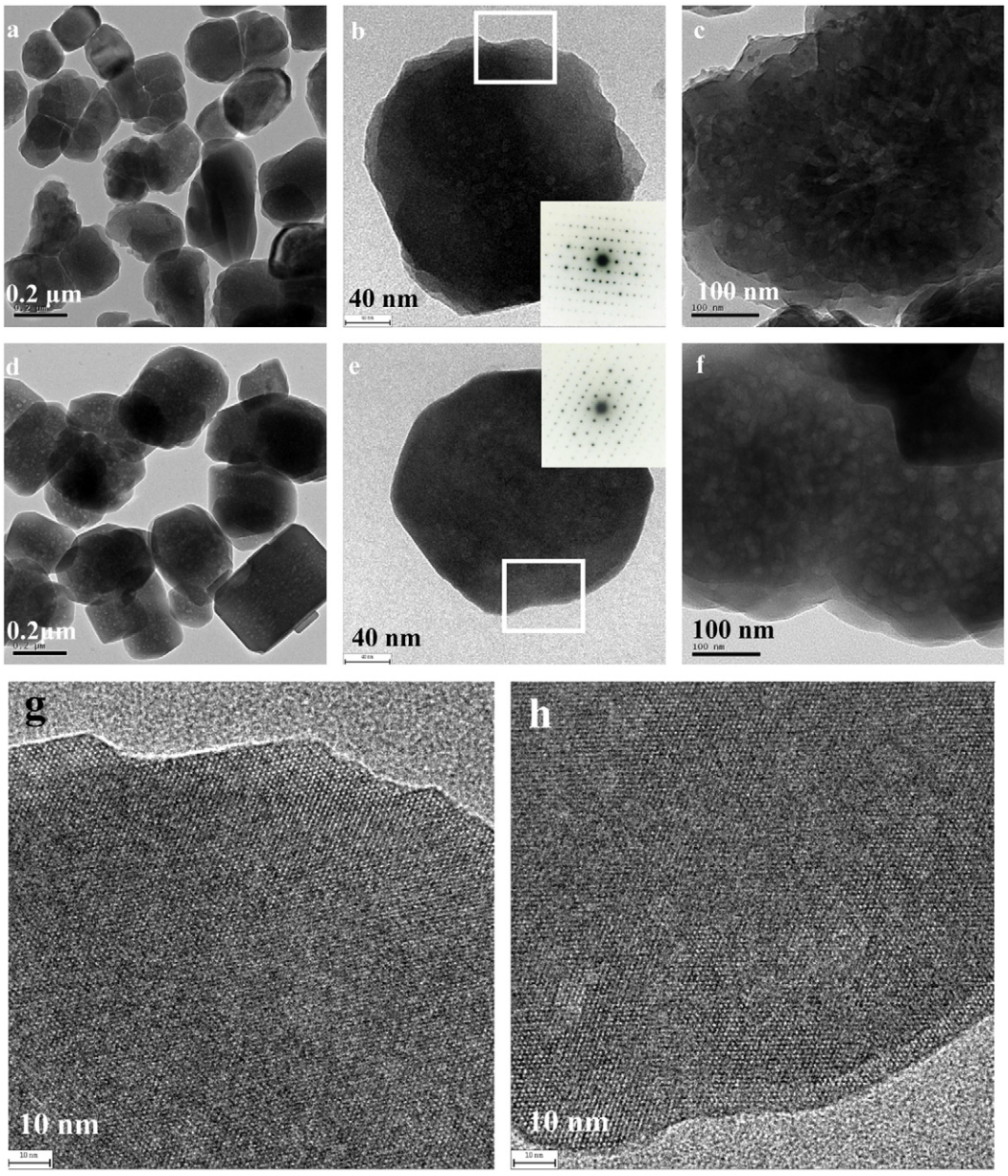

Fig. 7. TEM images of mesoporous MFI zeolites. (a, b) S-ZSM-5; (c) S-TS-1; (d, e) C-ZSM-5, (f) C-TS-1, and HR-TEM images (g, h) taken from the square frame in (b, e, respectively).

vibration of the pyridinium ion and has been used for the identification of the Brönsted acid sites. The other at about 1490 cm^{-1} is attributed to the pyridine species interacting with both the two kinds of acid sites. With increasing Si/Al ratio, the intensity of all bands decreases.

Acetalization of cyclohexanone and hydroxylation of phenol were performed to verify the catalytic activity of mesoporous ZSM-5 and mesoporous TS-1, respectively. The results are listed in Tables 2 and 3. It is found that the conversion of cyclohexanone on mesoporous ZSM-5 was increased with the increase of Al amount independent on S-ZSM-5 or C-ZSM-5, and a little bit higher than that on commercial ZSM-5 (designated as com-ZSM-5, Si/Al=25). But the selectivity to 1,1-dimethoxycyclohexane on mesoporous and commecial ZSM-5 are the same, ca. 92%. The similar selectivity would be attributed to the similar environment on mesoporous ZSM-5 and Com-ZSM-5 because all aluminum atoms are incorporated into the zeolite framework at 4-coordinate state and different porogens have no influence on the incorporation state of aluminum species. The little bit higher conversion of cyclohexanone on mesoporous ZSM-5 is attributed to the mesopores inside every single crystals, which made more active site accessible to substrate. But some closed pores are existed, so, zeolites with interconnected mesopores obtained via the proposed synthesis method is still desirable, which will be the subject of our further study.

For hydroxylation of phenol, the conversion of phenol on S-TS-1 is 24.7%, on C-TS-1 is only 13.7% under the identical reaction conditions, this maybe due to the mesopores in S-TS-1 are more accessible. Moreover, the selectivity to diphenol (catechol and hydroquinone) on S-TS-1 is higher than that on C-TS-1 (50.6% vs 20.6%). Benzoquinone, tar, etc. were detected in the final reaction mixture as the by-products. Diphenol selectivity is directly related to the microenvironment of titanium species in TS-1 zeolite [25], the amount of the extraframework Ti on C-TS-1 is a

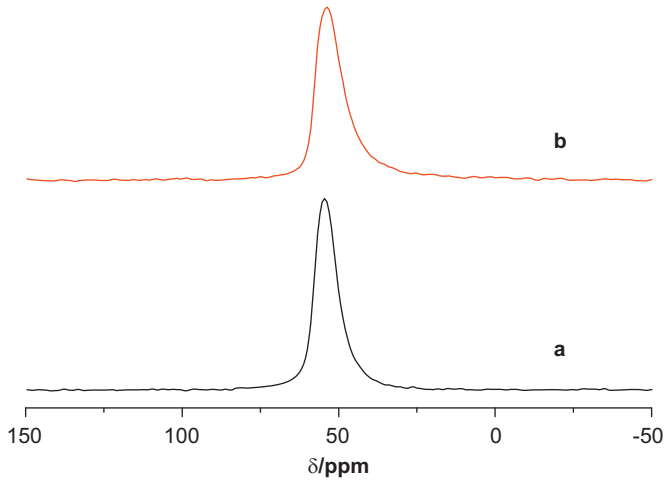

Fig. 8. ^{27}Al MAS NMR spectra of mesoporous ZSM-5: (a) S-ZSM-5 and (b) C-ZSM-5.

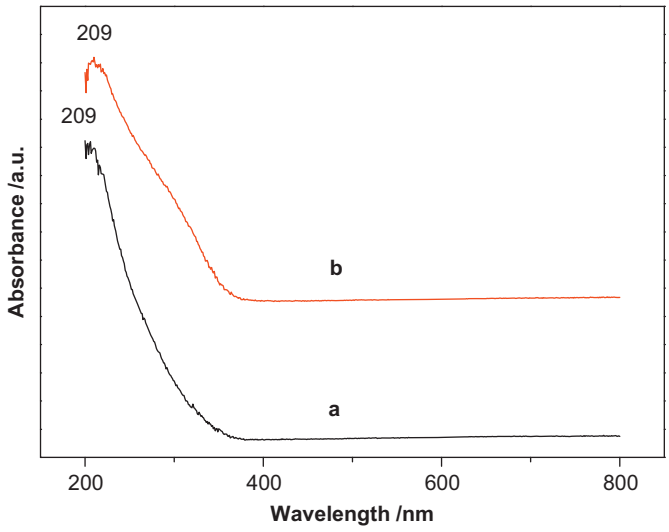

Fig. 9. UV–vis spectra of mesoporous TS-1: (a) S-TS-1 and (b) C-TS-1.

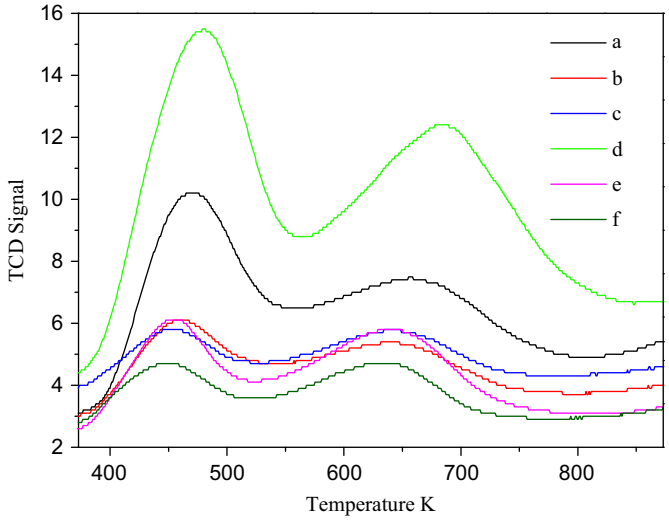

Fig. 10. NH_3-TPD of mesoporous ZSM-5 with various Si/Al molar ratios: (a) S-ZSM-5-20, (b) S-ZSM-5-50, (c) S-ZSM-5-100, (d) C-ZSM-5-20, (e) C-ZSM-5-50 and (f)S-ZSM-5-100.

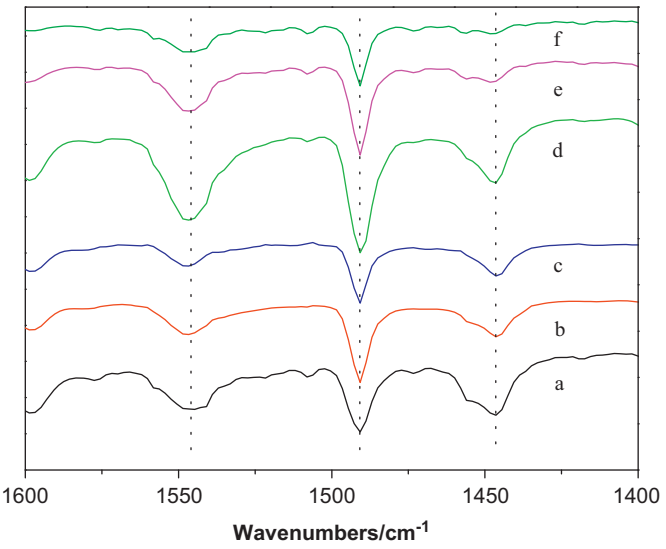

Fig. 11. Py-FT-IR spectra of mesoporous ZSM-5 with various Si/Al molar ratio obtained after adsorption of pyridine at 373 K: (a) S-ZSM-5-20, (b) S-ZSM-5-50, (c) S-ZSM-5-100, (d) C-ZSM-5-20, (e) C-ZSM-5-50 and (f) S-ZSM-5-100.

Table 2
Catalytic activity of mesoporous ZSM-5[a].

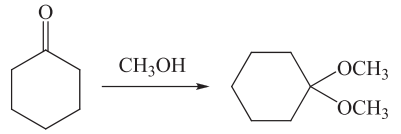

cyclohexanone 1,1-dimethoxycyclohexane

Catalyst (Si/Al)	S-ZSM-5			C-ZSM-5			Com-ZSM-5
	20	50	100	20	50	100	25
Conversion (%)	93.2	89.0	85.0	92.7	89.9	87.3	85.0

[a] The selectivity to 1,1-dimethoxycyclohexane in all the reactions is ca. 92%.

Table 3
Catalytic activity of mesoporous TS-1.

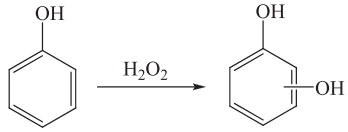

phenol diphenol

Catalyst (Si/Ti=40)	Phenol	
	Conversion (%)	Selectivity (%)
S-TS-1	24.7	50.6
C-TS-1	13.7	22.6

little bit more than that on S-TS-1, which may be lead to the lower selectivity to diphenol.

4. Conclusion

In summary, highly crystallized mesostructured MFI zeolite single crystals with different aluminum content have been synthesized by adding natural macromolecular polymers to a conventional hydrothermal synthesis system. The Si/Al ratio of the samples is tunable and nearly all of the Al atoms were located

at tetrahedral-coordinated sites in the framework. The prepared zeolites show high surface area and mesopores within zeolitic walls, these features are useful for applications in various fields, such as catalysis, adsorption and so on. Furthermore, this simple method could be easily extended to prepare other hierarchical structure zeolites, such as mesoporous TS-1. Importantly, the synthesis method reported in this paper is cost-effective and environmental friendly.

Acknowledgments

This project was supported financially by the 973 Program of China (2010CB732300), the National Natural Science Foundation of China (no. 20973058), the Commission of Science and Technology of Shanghai Municipality (10XD1401400) and the "Excellent scholarship" of East China University of Science and Technology, China.

References

[1] C.H. Christensen, K. Johannsen, I. Schmidt, C.H. Christensen, J. Am. Chem. Soc. 125 (2003) 13370–13371.
[2] M. Hartmann, Angew. Chem. Int. Ed. 43 (2004) 5880–5882.
[3] J. Pérez-Ramírez, C.H. Christensen, K. Egeblad, C.H. Christensen, J.C. Groen, Chem. Soc. Rev. 37 (2008) 2530–2542.
[4] R. Srivastava, M. Choi, R. Ryoo, Chem. Commun. 43 (2006) 4489–4491.
[5] Y. Tao, H. Kanoh, L. Abrams, K. Kaneko, Chem. Rev. 106 (2006) 896–910.
[6] K. Egeblad, C.H. Christensen, M. Kustova, C.H. Christensen, Chem. Mater. 20 (2008) 946–960.
[7] A. Corma, V. Fornes, S.B. Pergher, Th.L.M. Maesen, J.G. Buglass, Nature 396 (1998) 353–356.
[8] J.C. Groen, J.A. Moulijn, J. Pérez-Ramírez, J. Mater. Chem. 16 (2006) 2121–2131.
[9] J. Pérez-Ramírez, S. Abelló, A. Bonilla, J.C. Groen, Adv. Funct. Mater. 19 (2009) 164–172.
[10] C.J.H. Jacobsen, C. Madsen, J. Houzvicka, I. Schmidt, A. Carlsson, J. Am. Chem. Soc. 122 (2000) 7116–7117.
[11] I. Schmidt, A. Boisen, E. Gustavsson, K. Ståhl, S. Pehrson, S. Dahl, A. Carlsson, C.J.H. Jacobsen, Chem. Mater. 13 (2001) 4416–4418.
[12] A.H. Janssen, I. Schmidt, C.J.H. Jacobsen, A.J. Koster, K.P. de Jong, Micropor. Mesopor. Mater. 65 (2003) 59–75.
[13] Y. Tao, H. Kanoh, K. Kaneko, J. Am. Chem. Soc. 125 (2003) 6044–6045.
[14] W. Li, A. Lu, R. Palkovits, W. Schmidt, B. Spliethoff, F. Schüth, J. Am. Chem. Soc. 127 (2005) 12595–12600.
[15] A. Sakthivel, S. Huang, W. Chen, Z. Lan, K. Chen, T. Kim, R. Ryoo, A.S.T. Chiang, S. Liu, Chem. Mater. 16 (2004) 3168–3175.
[16] Z. Yang, Y. Xia, R. Mokaya, Adv. Mater. 16 (2004) 727–732.
[17] H. Wang, T.J. Pinnavaia, Angew. Chem. Int. Ed. 45 (2006) 7603–7606.
[18] F. Xiao, L. Wang, C. Yin, K. Lin, Y. Di, J. Li, R. Xu, D. Su, R. Schlögl, T. Yokoi, T. Tatsumi, Angew. Chem. Int. Ed. 45 (2006) 3090–3093.
[19] M. Choi, H.S. Cho, R. Srivastava, C. Venkatesan, D.H. Choi, R. Ryoo, Nat. Mater. 5 (2006) 718–723.
[20] B. Zhang, S.A. Davis, S. Mann, Chem. Mater. 14 (2002) 1369–1375.
[21] Y. Liu, W. Zhang, Z. Liu, S. Xu, Y. Wang, Z. Xie, X. Han, X. Bao, J. Phys. Chem. C 112 (2008) 15375–15381.
[22] L. Wang, C. Yin, Z. Shan, S. Liu, Y. Du, F. Xiao, Colloids Surf. A: Physicochem. Eng. Aspects 340 (2009) 126–130.
[23] P.L. Llewellyn, J.P. Coulomb, Y. Grillet, J. Patarin, G. Andre, J. Rouquerol, Langmuir 9 (1993) 1852–1856.
[24] J.C. Groen, J. Pérez-Ramírez, J. Appl. Catal. A 268 (2004) 121–125.
[25] F. Xiao, Y. Han, Y. Yu, X. Meng, M. Yang, S. Wu, J. Am. Chem. Soc. 124 (2002) 888–889.